Low temperature sintering of CaZrO3 using lithium fluoride addition

Michaël Pollet, Sylvain Marinel

Low temperature sintering of $CaZrO_3$ using lithium fluoride addition

M. Pollet*, S. Marinel

CRISMAT Laboratory, UMR 6508 CNRS/ISMRA, 6 Bd du Mal Juin 14050 Caen, France

Abstract

The effects of lithium fluoride on the sinterability, the microstructure and the low frequency dielectric properties of acceptor/donor doped $CaZrO_3$ ceramics were investigated. The acceptor(Mn)/donor(W) doping was used to avoid $CaZrO_3$ reduction. Lithium fluoride was selected as a liquid phase sintering aid to lower the sintering temperature. The dielectric properties of $CaZrO_3$ ceramics with LiF additions are strongly dependent on the densification, the microstructure, and the reaction with LiF. $CaZrO_3$ ceramics without LiF addition sintered at high temperature display a high permittivity, low losses and a good behavior under an electrical field as a function of temperature. Using LiF, this dielectric can be sintered at 1000 °C to achieve theoretical densities of 91%, ε_r values of 31 and losses close to 0.4%. This low sintering temperature allows co sintering with base metal, nickel and copper, for which scanning electron microscopy and energy dispersive spectroscopy results are presented.

Keywords: Base metal electrodes; Capacitors; $CaZrO_3$; LiF; Multilayer capacitors; Sintering

1. Introduction

The multilayer ceramic capacitor (MLCC) market has been growing in pace with the exponential development of the communications technologies. Almost half of this production is based on noble metal electrodes (Pt, Pd, Ag) which are expensive and the development of cheaper base metal electrode MLCC (BME-MLCC) is more and more studied.

The aim of this work is to discuss the feasibility of preparing a type I BME-MLCC with a high dielectric permittivity, manufactured with nickel or copper inner-electrodes.

The dielectric material chosen for this study is the $CaZrO_3$ perovskite. This material has recently been studied for its high performance as an ionic conductor for solid electrodes in fuel cells.[1,2] $CaZrO_3$ ceramics have a relatively high permittivity (25–30), low losses and a high insulation resistance.[2–4]

The manufacture of BME-MLCC presents essentially two problems: first, the base metals used in the cofiring process (generally Ni, possibly Cu), are sensitive to oxidation, and the final component must therefore be fired in a reducing atmosphere. Second, these metals have low melting points (1453 °C for Ni and 1083 °C for Cu), which requires a decrease in the sintering temperature of the dielectric (which is usually around 1550 °C). The first point has been extensively studied, especially in the case of $BaTiO_3$, to make it co-sinterable with nickel electrodes. In this system, the transition metal in the oxide is easily reduced to form Ti^{3+}/Ti^{2+} ions, which induce oxygen vacancies and give rise to poor insulating resistance. It is then necessary to compensate for this by introducing acceptor dopants.[5–9] The same behaviour is observed in other Ti based dielectrics such as $MgTiO_3$.[10] Even if a zirconate is less sensitive to reduction,[11,12] the decision has been taken here to use an acceptor/donor complex as in $BaTiO_3$ ceramics. The second point, i.e. the lowering of the sintering temperature has also been considered. For this important point, the effect of LiF addition on the sintering of $CaZrO_3$ has been tested. It is indeed well known that such additions often make it possible to decrease the sintering temperature of perovskite materials.[13,14]

This study of $CaZrO_3$ is divided in three parts: (i) the sintering process at low temperature with the analysis of

* Corresponding author.
E mail address: michael.pollet@ismra.fr (M. Pollet).

the addition of lithium fluoride; (ii) the effect of a reducing atmosphere on the dielectric material; and (iii) the Cu or Ni-cofired sample characterisation.

2. Experimental procedures

First, a 1 at.% Zr-deficient $CaZrO_3$ phase was prepared using reagent grade (CERAC) $CaCO_3$ (99.95% purity) and ZrO_2 (99.95% purity). This non-stoichiometry is justified by the need to create vacancies to facilitate the insertion of the doping elements in the structure. These two powders were wet-ball-milled in ethanol for 45min. using an agate mortar with agate balls. The mixture was dried under infrared lamps and manually de-agglomerated in an agate mortar. This mixture was calcined in a tubular furnace (PIROX) at 1000 °C for a 2 h dwell with a 150°/h heating/cooling rate.

Next, the acceptor/donor doping agents (respectively MnO_2 and WO_3), were both added to this phase to 0.5 at.% each to strictly compensate the zirconium deficiency. The LiF addition was then carried out for several contents, namely 0, 0.5, 1, 2, 5, 10, 20, 30, 40 and 50 at%. These samples are named CZ_1LiF_y where the subscript "1" refers to the zirconium 1 at.% deficiency and the subscript "y" refers to the LiF addition content expressed in percent. This last mixture ($CZ1 + 0.5\ WO_3 + 0.5\ MnO_2 + y$ LiF) was wet-ball-milled in ethanol for 45 min. using an agate mortar with agate balls. Once again, the mixture was dried under infrared lamps and manually de-agglomerated in an agate mortar. The powders were then granulated with an organic binder and uniaxially pre-compacted to form green discs. The 6.36 mm∅ discs for dilatometric measurements were pressed under a load of 2100 kg. The 8.06 mm∅ discs for sintering were pressed under a load of 3880 kg.

In order to investigate the influence of these additions on the resulting phase composition, all of the synthesised powders and discs were analysed by X-ray diffraction either with a Guinier camera (ENRAF NONIUS FR590) or with a SEIFERT diffractometer (Copper $K\alpha_1$ radiation).

Dilatometric measurements were carried out in static air using a SETARAM TMA92 dilatometer. For all the measurements, the samples were heated and cooled at 2°/min with a dwell at 1350 °C for 1 h. A slight load of 1 g was applied to allow the measurements.

A heat/cool ramp of 2.5°/min was chosen for the sintering in a tubular furnace, with a thermal cycle dependent upon the BME studied. Nevertheless, the dwell time was systematically 6 h, whatever the dwell temperature used. The sintering atmosphere was air (static) or a mixture composed of 10%H_2/90% Ar, moisture saturated at room temperature (RT).

The co-fired sample were prepared using in each case two 8.06 mm∅ discs (around 1 mm thickness). One face of each was painted with a mix of either nickel or copper powder and organic binder. The painted faces were placed facing each other and the two discs were pressed together under a load of 3880 kg. When using base metal as the inner electrode, the atmosphere for sintering was 10%H_2/90% Ar to avoid the metal oxidation. The sintering temperature was either 1350 °C (for nickel electrodes) or 1000 °C (for copper electrodes). A dwell time of 6 h was imposed and the heating rate was 2.5 K/min.

The polished samples were observed under a polarised optical microscope (Olympus BH2-HLSH) or, after gold-sputtering, by using a scanning electron microscope (Philips XL30 FEG SEM).

Phase composition analysis was determined by using an energy dispersive spectrometer coupled with the SEM (EDS - Oxford Link ISIS). Quantitative analysis was carried out by atomic absorption using a VARIAN SpectrAA-20 spectrometer.

Electrical measurements were realized on shaped discs painted on both faces with an In-Ga eutectic paste and dried in an oven at 120 °C. Insulating resistance measurements were obtained using a SEFELEC DM500A megohmmeter and the dielectric characteristics [ε, $tg(\delta)$] were acquired at 1 MHz with a FLUCKE 6306 LCR meter.

3. Results and discussion

First will be related the effect of the acceptor/donor doping agent and of the 1 at.% zirconium-deficiency on the dilatometric curves. The dilatometric measurements show that the CZ_1LiF_0 (i.e. the sample to which only manganese and tungsten are added) shrinks at lower temperature than the stoichiometric phase $CaZrO_3$ [CZ_0] (Fig. 1 a). Further experiment pointed out that this behaviour was only due to the zirconium deficiency (Fig. 1b). Indeed, considering only the 1 at.% zirconium-deficient phase CZ_1 (no added doping agent), one can see that its shrinkage curve coincides more or less with that of CZ_1LiF_0. Moreover, trials realised with CZ_1 and different combinations of the doping agents (Fig. 1b) show that their only effect is either no shift of the sintering temperature (Mn) or an increase of 200 K for the temperature at the maximum shrinkage rate (W). Additional experiments are being carried out to confirm the effect of the stoichiometry and will be published elsewhere. Nevertheless, a first interpretation of this result can be made in term of facilitated diffusion through the deficient lattice.

Let us now consider the effect of the lithium fluoride addition. The curves of the dilatometric measurements and their derivative curves are respectively shown in Fig. 2a and b. An effect can be observed even for a small amount of LiF but not in the desired way. The

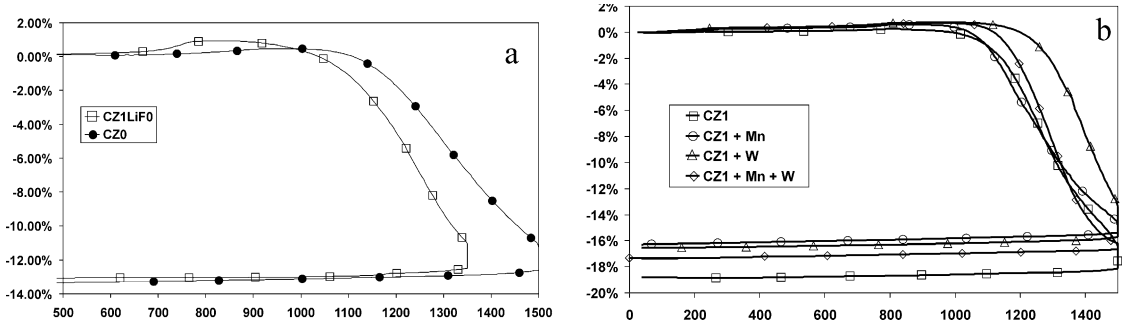

Fig. 1. Dilatometric results of a) CZ0 and CZ_1LiF_0 and b) CZ_1, CZ_1 + Mn, CZ_1 + W and CZ_1 + Mn + W.

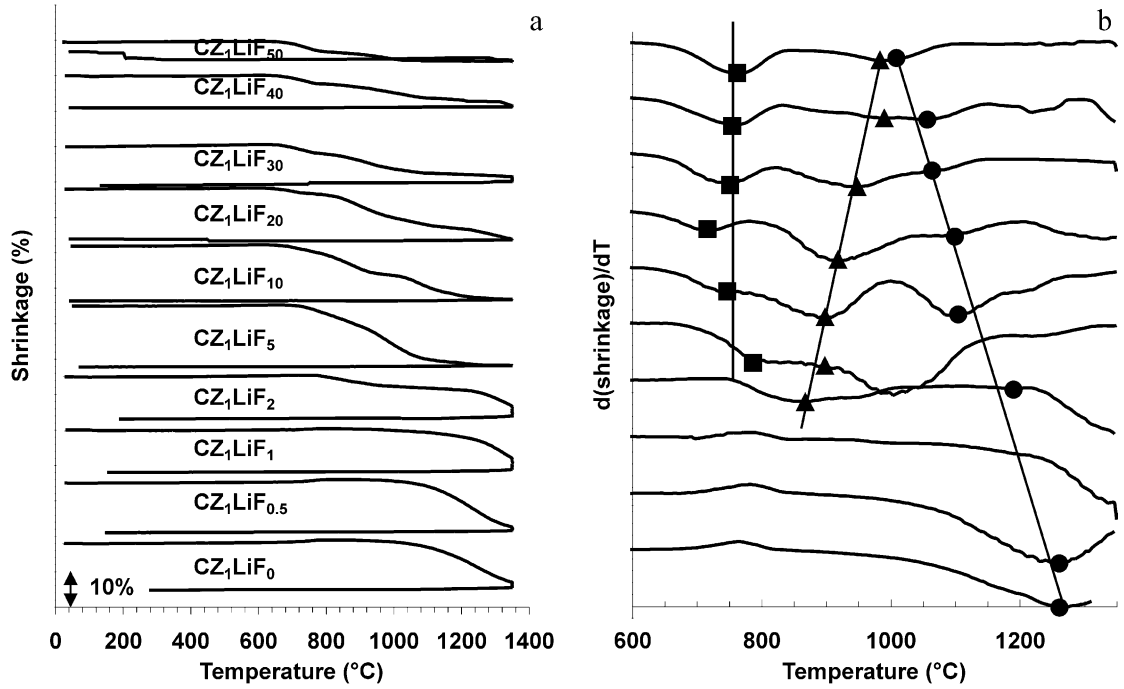

Fig. 2. (a) Dilatometric measurements curves of CZ_1LiF_y and (b) their derivative curves.

$CZ_1LiF_{0.5}$ only exhibits an increase of the shrinkage (×1.5) as can be seen on the derivative curves. The CZ_1LiF_1 displays the worst behaviour with a shift to higher temperature of more than 100 K of the shrinkage maximum. From 2 at.% LiF addition, new effects near 860 °C can be observed from the derivative curves as is highlighted on Fig. 2b. As LiF addition increases, these lower temperature mechanisms split in two. The one appearing at the lowest temperature is centred at around 750 °C (see the squares on Fig. 2b). The second mechanism's average temperature moves with increasing LiF content from nearly 850 to 1000 °C, these temperature being taken at the maximum shrinkage rate on the derivative curves (triangles on Fig. 2b). The third effect corresponds to the CZ_1LiF_0 mechanism initially at temperature near 1250 °C shifting for higher LiF additions to lower temperature to nearly merge with the second mechanism at around 1000 °C (full circles in Fig. 2b). These behaviours are evidenced in Fig. 2b with straight lines.

The first mechanism (nearly centred at 750 °C) is consistent with the existence of the eutectic [80% LiF;20% CaF_2] for which the melting temperature is 769 °C. The slight shift of the temperature could arise from either the doping agents or from the thermal process. The second mechanism, first observed at 850 °C with CZ_1LiF_2 is in excellent agreement with the LiF melting point (T_f = 845 °C). Finally, the third one coincides, as already presented, with the CZ_1LiF_0 standard shrinkage process.

As LiF additions increase, the first mechanism is favoured with a facilitated formation of the eutectic and for the most modified samples ($\geqslant$40%), it tends to become the only one. In contrast, for additions around 10% LiF, the second mechanism is dominating the first one before slowly disappearing for higher LiF rates. Finally, the third one decreases from no LiF addition to

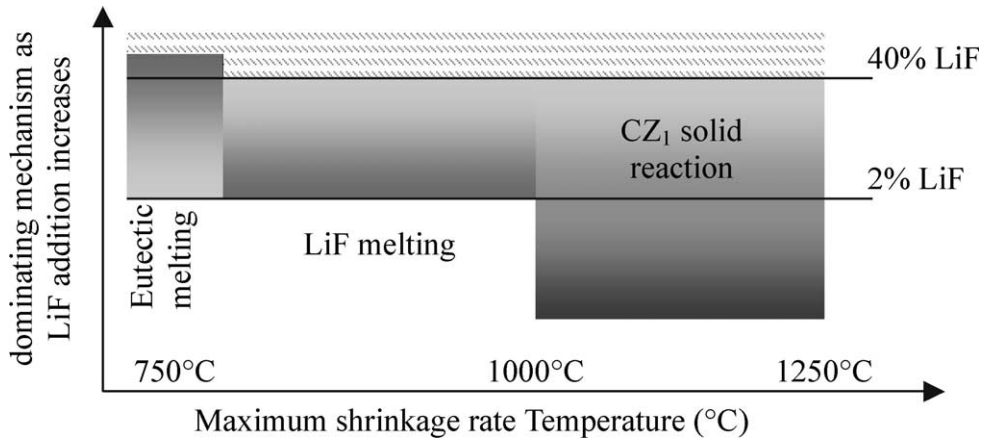

Fig. 3. Shrinkage mechanism's temperature's domain.

the 50% LiF addition sample. The influence of the temperature domain on these mechanisms is summarised in Fig. 3.

As is clearly visible in Fig. 2a, as the LiF addition increases, the shrinkage diminishes. In order to estimate the influence of LiF addition on the final densities, the data have been used to plot the percentage of the theoretical density attained versus temperature. Considering the shrinkage to be isotropic, and the sample weight to be constant and equal to the final one ($m = m_{\text{initial}} - m_{\text{organic binder}} - m_{\text{lithium salt}}$), the relative density is evaluated as:

$$\%d = \frac{m}{V_0 \cdot (1+\varepsilon)^3 \cdot d_{\text{th}}}$$

V_0 being the initial volume of the disc, ε the shrinkage in percent and d_{th} the theoretical density of the material. This parameter was calculated assuming that the lithium salt addition does not remain in the material as was suggested by weight losses and confirmed by atomic absorption measurements and that the doping agents (Mn and W) enter the B site in the ABO_3 structure. As the relative density curves have the same profile as the shrinkage ones, only the analysis results are shown. Fig. 4 shows the temperature required to reach a particular density (here from 70 to 95% of the theoretical value with 5% step) as a function of LiF additions. This simple representation makes it possible to observe rapidly the effect of the addition: firstly, the earliest efficient behaviour is obtained with a 10% LiF addition

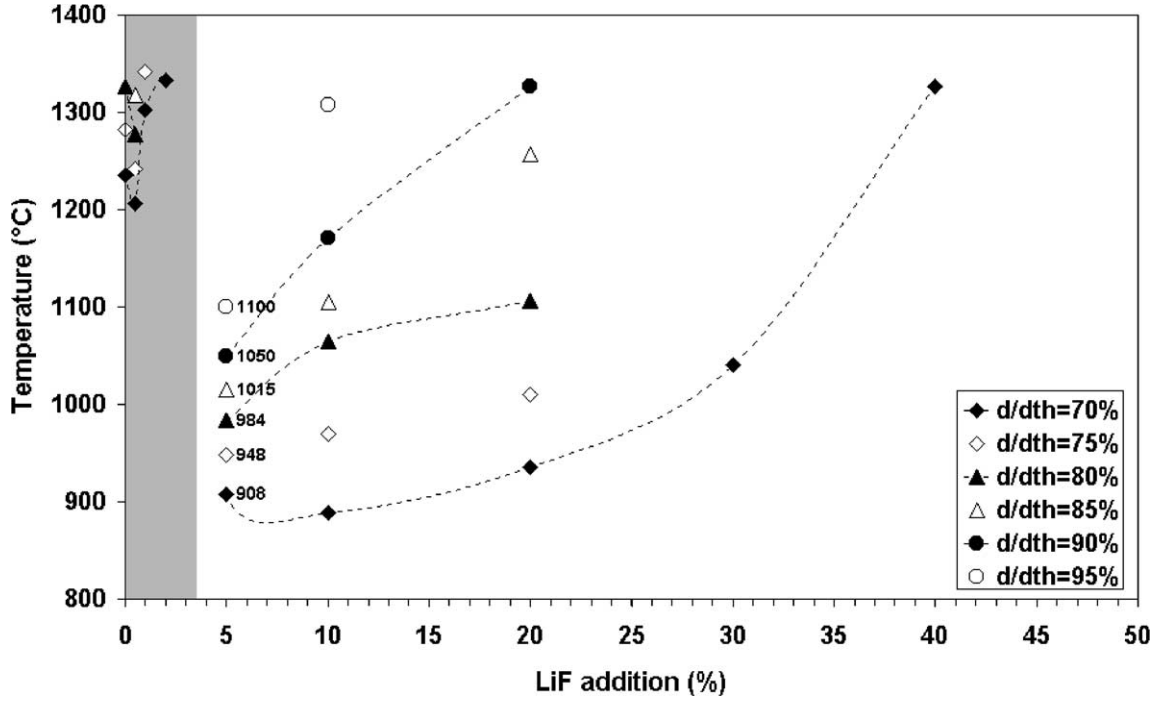

Fig. 4. Temperature to reach to obtain a particular density as a function of LiF content.

for which the sample reaches 70% of the theoretical density below 890 °C; secondly, the figure clearly evidences an optimum with 5% LiF addition with a sample reaching high densities ($\geqslant$75% of the theoretical one) faster than any other samples and attaining 95% of the theoretical density at 1100 °C, that is to say a gain of more than 450 °C compared to the undoped stoichiometric $CaZrO_3$ ceramic ($T_{sintering} \approx$1550–1600 °C). Nevertheless, except for these two notable results, one can see that LiF additions below 5% or above 10% seem to be inefficient. Below 5% LiF additions, none of the tested compositions reach highly densified states since, in the temperature domain tested, only the 0.5% LiF sample managed to reach 90% of the theoretical density after a dwell at 1350 °C. In the same way, above 10% LiF, only CZ_1LiF_{20} reached 90% of the theoretical density at a temperature slightly below 1350 °C.

The apparent densities calculated from the geometrical and weight measurements after the sintering treatment using the dilatometer are reported in Table 1. These results are in good agreement with the dilatometric observations. The better sintered mixtures are the $CZ_1LiF_{0.5–5–10}$ with relative densities higher than 90%. The two last results were clearly predicted by the dilatometric measurements whereas the first one (0.5% LiF) as mentioned earlier is more unexpected. These three efficient compositions coincide with the three least uneven dilatometric curves, i.e. the ones for which the shrinkage rates remain relatively linear or constant. This seems to indicate that a step-by-step sintering is unfavourable for densification.

3.1. Sintering at intermediate temperature (1350 °C)

Considering the poor results obtained in the dilatometric analysis for extreme values of LiF addition, all the samples except those with LiF addition >20% were sintered at 1350 °C with a dwell of 6 h to try to enhance densification. Both sintering atmosphere were alternatively used, i.e. static air or a mixture of 10% H_2/90% Ar, moisture saturated at room temperature (RT). First will be discussed the results obtained by sintering in static air atmosphere. Whatever the sample, no secondary phase is observed using X-ray diffraction. The relative densities obtained are reported in Table 2. Except for small LiF addition, i.e. $\leqslant$0.5%, and the CZ_1LiF_5 sample, the results are in good agreement with the dilatometric measurements. The shift for the above-mentioned samples is due both to the different shapes of the samples, to the furnace configuration which does not radiate as much as that used for the dilatometer and of course the load imposed for the dilatometric measurements. Photographs of the microstructures of the denser samples are shown on Fig. 5. They corresponds to the measured densification of nearly 85–90% for these samples. Higher magnification also shows the remaining pore channels in the CZ_1LiF_1 sample whereas the $CZ_1LiF_{10–20}$ samples are more densified (less pore channels) and contain more closed porosity. The CZ_1LiF_{10} grain diameter is around 500 nm whereas the CZ_1LiF_{20} grains have coarsened to around 1 μm. The weight losses account for the total removal of the lithium salt which was confirmed using atomic absorption measurements. Finally, the electric and dielectric measurements (Table 2) show that the results are within the uncertainty of the measurements, independent of LiF addition.

Further observations were made on samples sintered under the same conditions except for the atmosphere which was now the 10%H_2/90% Ar mixture. Here again, X-ray diffraction indicated no secondary phases. Table 3 reports the results obtained and Fig. 6 shows the corresponding microstructures. Densities gain between 5 and 10% using this atmosphere. The considered explanation is simply the reduction of at least one of the ions, most probably the manganese, which enhances its mobility in the structure. The microstructures of the polished samples

Table 1
Geometric measurements of $CZ1LiF_y$ samples densities after dilatometric analysis

Sample	CZ_1LiF_0	$CZ_1LiF_{0.5}$	CZ_1LiF_1	CZ_1LiF_2	CZ_1LiF_5	CZ_1LiF_{10}	CZ_1LiF_{20}	CZ_1LiF_{30}	CZ_1LiF_{40}	CZ_1LiF_{50}
%d	90%	**93%**	88%	84%	**94%**	**92%**	88%	77%	68%	67%

Table 2
Geometric, dielectric and electric measurements of CZ_1LiF_y samples sintered in static air at 1350 °C

Sample	CZ_1LiF_0	$CZ_1LiF_{0.5}$	CZ_1LiF_1	CZ_1LiF_2	CZ_1LiF_5	CZ_1LiF_{10}	CZ_1LiF_{20}
%d (±3)[a]	80%	81%	90%	80%	78%	92%	85%
ε (±3)	29	26	30	28	26	34	30
$tg(\delta)$	0.1%	3.3%	2.0%	0.7%	0.3%	0.3%	0.4%
$\log(\rho_i$ [Ω.cm]) (±1)	10	10	11	10	10	10	10

The error noted into brackets only derives from the uncertainty of measurements devices.
[a] %d Is the percentage of the theoretical density, ε, $tg(\delta)$ and ρ_i have their standard meaning.

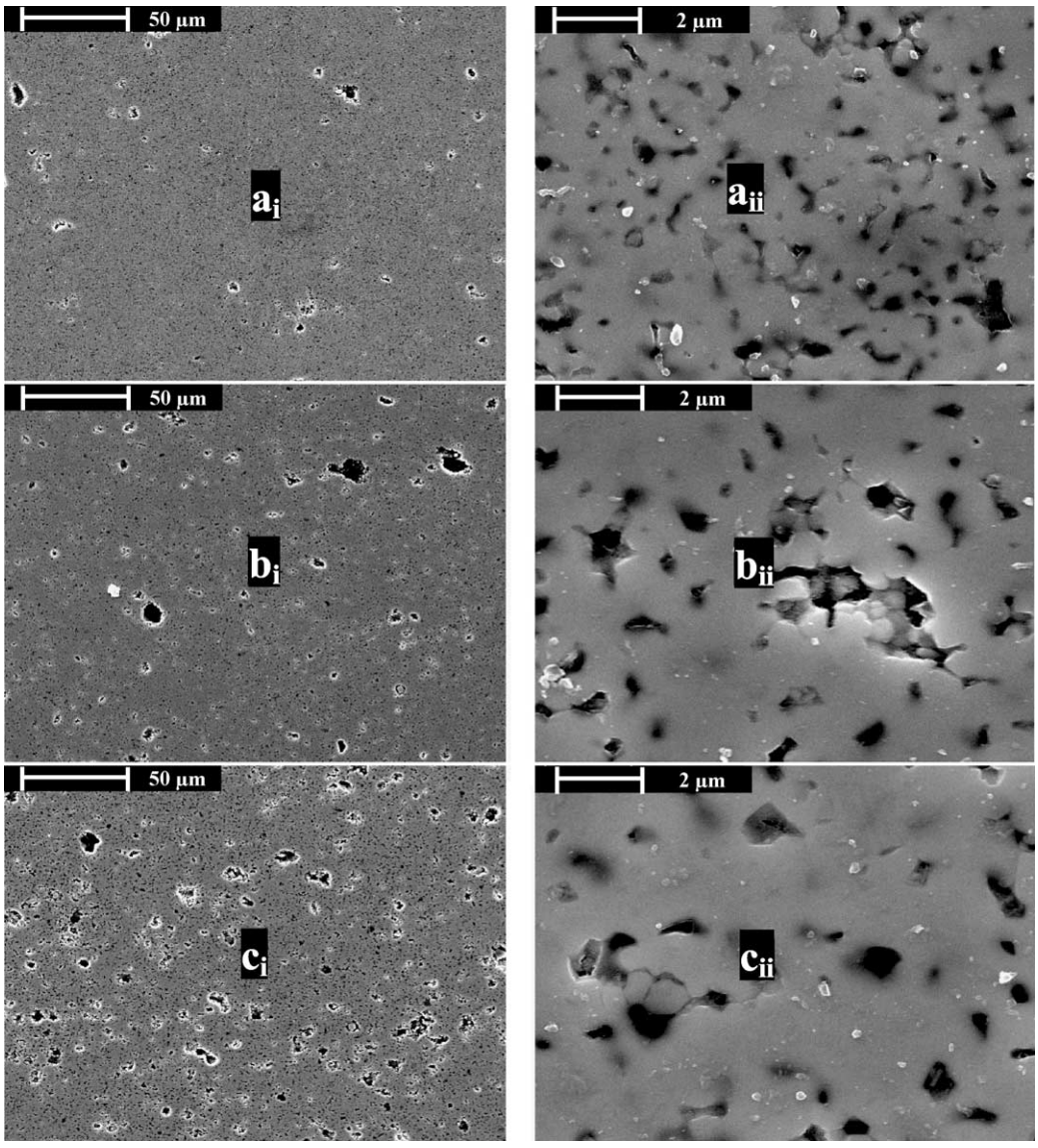

Fig. 5. Microstructures of 1350 °C/static air sintered polished samples. (a) CZ_1LiF_1; (b) CZ_1LiF_{10}; (c) CZ_1LiF_{20} (subscript: i ×400 magnification; ii ×8000 magnification).

Table 3
geometric, dielectric and electric measurements of CZ_1LiF_y samples sintered in the 10% H_2/90% Ar mixture at 1350 °C

Sample	CZ_1LiF_0	$CZ_1LiF_{0.5}$	CZ_1LiF_1	CZ_1LiF_2	CZ_1LiF_5	CZ_1LiF_{10}	CZ_1LiF_{20}
$\%d$ (±3)[a]	89%	92%	97%	92%	92%	95%	96%
ε (±3)	34	27	37	29	36	36	30
$tg(\delta)$	9.4%	4.0%	0.2%	1.1%	0.1%	0.3%	0.4%
$\log(\rho_i$ [Ω.cm]) (±1)	11	10	10	11	11	10	10

The error noted into brackets only derives from the uncertainty of measurements devices.
[a] $\%d$ Is the percentage of the theoretical density, ε, $tg(\delta)$ and ρ_i have their standard meaning.

look like those of the air sintered samples, but the fracture surfaces confirm the high densities reported in Table 3. The grain diameters are respectively 1, 1 and nearly 2 µm for 1, 10 and 20% LiF additions. Owing to the results reported in Table 3, the permittivities seem slightly increased whereas the dielectric losses seem to decrease as the LiF content increases. These results are certainly due the densification enhancement, the most significant shift being observable on the samples showing the most important difference in densities for the two different atmospheres used. Finally, the insulating resistivities seem to be independent of the atmosphere.

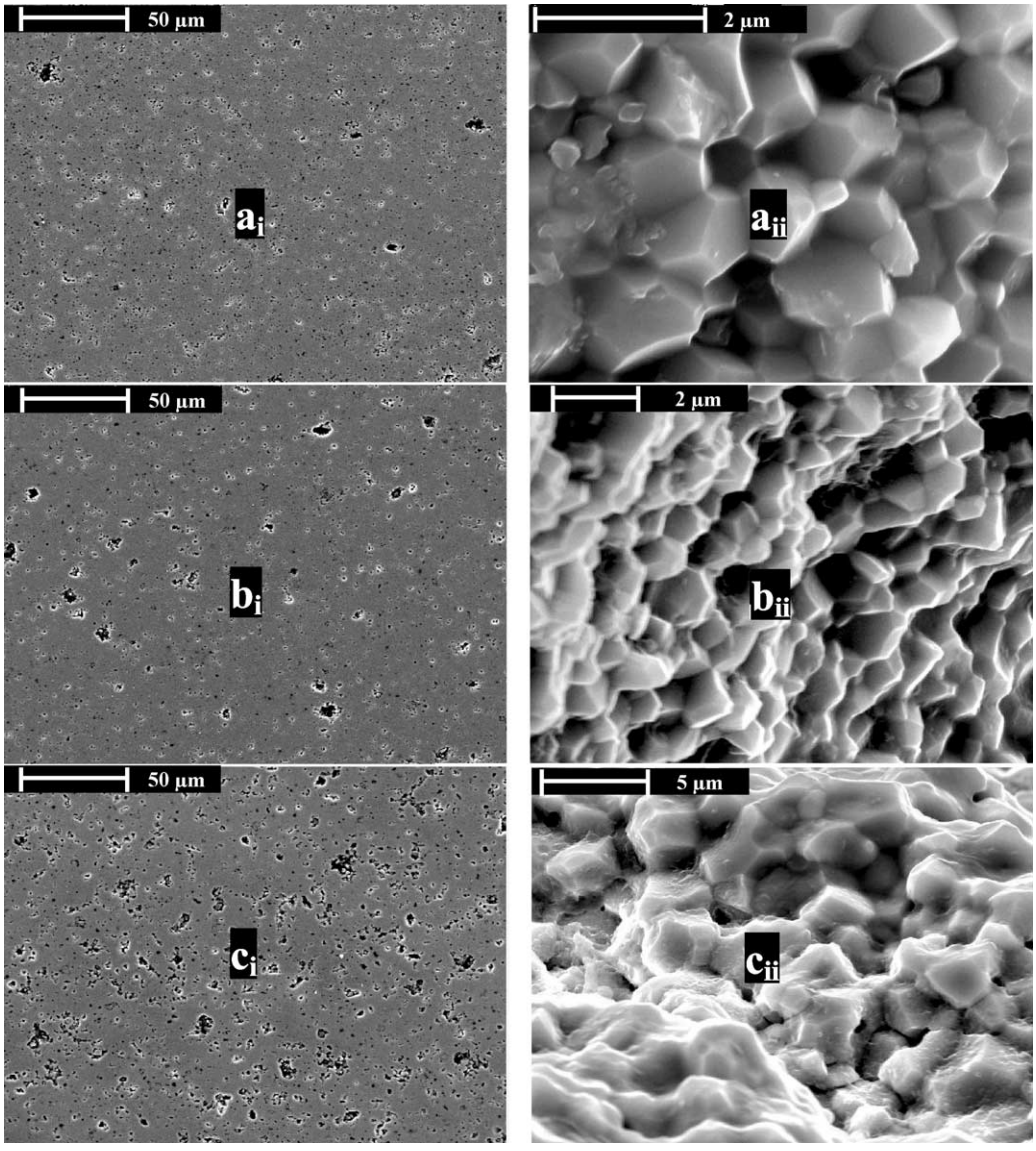

Fig. 6. Microstructures of 1350 °C 10% H_2/90% Ar mixture sintered polished samples. (a) CZ_1LiF_1; (b) CZ_1LiF_{10}; (c) CZ_1LiF_{20} (subscript:i ×400 magnification; ii fractured samples, non constant magnification).

3.2. Sintering at low temperature (1000 °C) in the 10% H_2/90% Ar mixture

Only the $CZ_1LiF_{5–10–20}$ samples which sinter at lower temperature are considered, i.e. those which have strong low temperature modes on the shrinkage derivative curves (%LiF addition $\leqslant 5$) and which have good shrinkage at higher temperature (%LiF addition $\geqslant 20$). The results are reported in Table 4 and Fig. 7 shows the microstructure of the best sintered sample (CZ_1LiF_{10}). Fig. 7a evidences a well sintered ceramic, accounting for the measurement of 91% of the theoretical density. The observation of a dense fractured area (Fig. 7b) reveals a well structured material with clearly joined grains of nearly 350 nm diameter. This sample has also interesting electric and dielectric properties with a permittivity around 31, low losses (≈0.4%) and a suitable insulating resistivity. The other two samples are less satisfactory. The CZ_1LiF_5 only reaches 78% of the theoretical density. This low densification behaviour is understandable considering its shrinkage derivative curve which displays the major contribution of the high temperature

Table 4
Geometric, dielectric and electric measurements of CZ_1LiF_y samples sintered in the 10% H_2/90% Ar mixture at 1000 °C

Sample	CZ_1LiF_5	CZ_1LiF_{10}	CZ_1LiF_{20}
%d (±3)	78%	91%	90%
ϵ (±3)	NM	31	NM
$tg(\delta)$	NM	0.4%	NM
log(ρ_i [Ω.cm]) (±1)	9	11	9

The error noted into brackets only derives from the uncertainty of measurements devices NM not measurable. d Is the percentage of the theoretical density, ε, $tg(\delta)$ and ρ_i have their standard meaning.

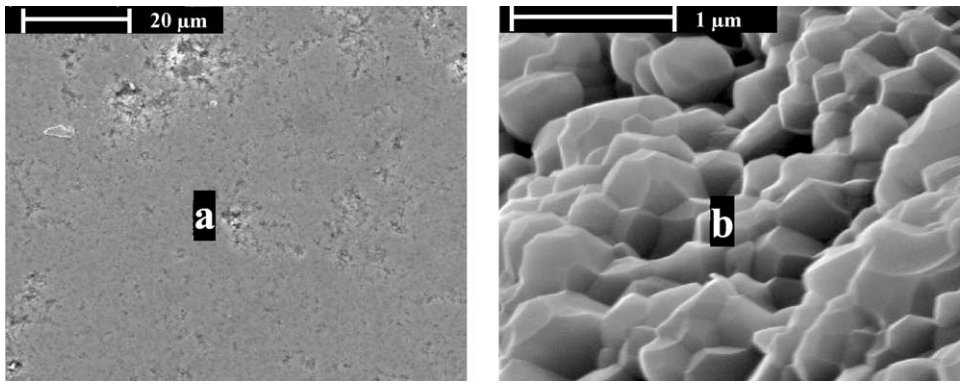

Fig. 7. Microstructures of CZ_1LiF_{10} sintered at 1000 °C in a 10% H_2/90% Ar mixture (a) polished sample (×2000) (b) fractured sample (×60,000).

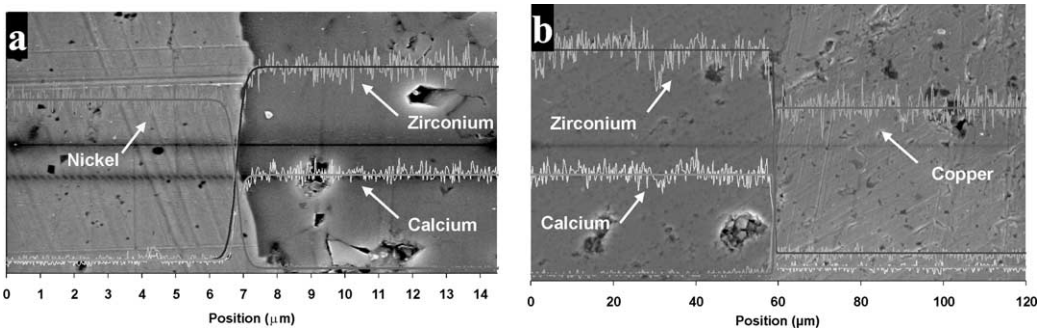

Fig. 8. Microstructures and EDS analysis of the interface of the co sintered CZ_1LiF_{10} with (a) nickel at 1350 °C (b) copper at 1000 °C.

shrinkage mechanism. Owing to this poor result, the dielectric properties are not measurable. The CZ_1LiF_{20} reaches 90% of the theoretical density, but its dielectric properties are too poor to be measured. All three samples are moreover highly dependant on the humidity conditions. Indeed, none of dielectric properties (nor electric) are measurable if the samples are not first dried. This last point may be a serious obstruction to applications if it is not solved; however, no further experiments have yet been done to overcome this drawback.

3.3. Co-sintered samples (nickel or copper)

As a result of the above experiments, the CZ_1LiF_{10} composition is chosen to synthesise the co-fired samples. Fig. 8 shows both the microstructures and the EDS analysis results obtained along a line crossing the interface ceramic/metal. In both cases, the photograph indicate clean interfaces and the EDS analysis suggests no diffusion between the different layers (i.e. no diffusion from metal to ceramic or vice versa). The EDS measurement threshold is 1 µm and, given this limit, one can say that no detectable diffusion occurs at the interface.

4. Conclusion

The addition of LiF decreases the sintering temperature of $CaZrO_3$ by introducing additional densification mechanisms. The lowest temperature behaviour is attributed to the formation of a [CaF_2;LiF] eutectic which melts at around 750 °C. In spite of numerous experiments, it was not possible to properly exploit this mechanism to allow a complete and full densification of the ceramic. The second mechanism is due to the LiF melting at 845 °C. It allows, combined with the first one, a densification at low temperature (1000 °C) for appropriate lithium salt addition. Finally, a third mechanism arises in calcium zirconate itself and appears at higher temperature.

The effect of the sintering atmosphere was also investigated. It is shown that a reducing atmosphere enhances the densification and thus slightly improves the electric and dielectric properties. This behavior is attributed to the manganese reduction.

Based on both the lowering of the sintering temperature and the non prejudicial effect of the atmosphere, co-sintered samples with the [$CaZrO_3$; Mn/W doped; LiF addition] system and either nickel or copper electrodes were synthesized. In both cases, the results suggest compatibility of the ceramic with the base metal.

Acknowledgements

The authors wish to thank the TEMEX Society for collaborating with us and allowing us to publish this work.

References

1. Engelen, W., Buekenhoudt, A., Luyten, J. and De Shutter, F., Humidity sensitivity of electrochemical hydrogen cells using cal cium zirconate ceramics. *Solid State Ionics*, 1997, **96**, 55 59.
2. Kiyoshi, Kobayashi, Shu, Yamaguchi and Yoshiaki, Iguchi, Electrical transport properties of calcium zirconate at high tem perature. *Solid State Ionics*, 1998, **108**, 355 362.
3. Yamagushi, T., Komatsu, Y., Otobe, T. and Murakami, Y., Newly developed ternary (Ca,Sr,Ba) zirconate ceramic system for microwave resonators. *Ferroelectrics*, 1980, **27**, 273 276.
4. Borglum, B.P. and Buchanan, R.C., SEM determination of opti mum processing conditions for microwave dielectrics in the (Ca,Sr,Ba) zirconate system. In *Proceedings of the 45th Annual Meeting of the Electron Microscopy Society of America, San Francisco Press*, ed. G.W. Bailey. 1987, pp. 372 373.
5. Albertsen, K., Hennings, D. and Steiglemann, O., Donor acceptor charge complex foration in barium titanate ceramics: role of firing atmosphere. *J. Electroceramics*, 1998, **2**(3), 193 198.
6. Hansen, P., Hennings, D. and Schreinemacher, H., Dielectric properties of acceptor doped (Ba,Ca)(Ti,Zr)O_3 ceramics. *J. Elec troceramics*, 1998, **2**(2), 85 94.
7. Hansen, P., Hennings, D. and Schreinemacher, H., High K dielec tric ceramics from donor/acceptor codoped ($Ba_{1\ x}Ca_x$)($Ti_{1\ y}Zr_y$)O_3 (BCTZ). *J. Am. Cer. Soc*., 1998, **81**(5), 1369 1373.
8. Lee, W. H., Tseng, T. Y. and Hennings, D., Effects of calcination temperature and A/B ratio on the dielectric properties of (Ba,Ca)(Ti,Zr,Mn)O_3 for multilayer ceramic capacitors with nickel electrodes. *J. Am. Cer. Soc*., 2000, **83**(6), 1402 1406.
9. Lee, Wen His, Tseng, Tseung Yuen and Hennings, D., Effects of A/B cation ratio on the microstructure and lifetime of ($Ba_{1\ x}$ Ca_x)z($Ti_{0,99\ y}Zr_yMn_{0,01}$)O3 (BCTZM) sintered in reducing atmo sphere. *J. Mat. Sci.: Mater. in Electronics*, 2000, **11**, 157 162.
10. Vigreux, C., Deneuve, B., El Fallah, J. and Haussonne, J. M., *J. Eur. Cer. Soc*., 2001, **21**(10 11), 1681 1684.
11. Davies, R. A., Islam, M. S. and Gale, J. D., Dopant and proton incorporation in perovskite type zirconates. *Solid State Ionics*, 1999, **126**, 323.
12. Nadler, M. R. and Fitzsimmons, E. S., Preparation and proper ties of calcium zirconate. *J. Am. Cer. Soc*., 1995, **38**(6), 214 217.
13. Haussonne, J.M., Regreny, O., Lostec, J., Desgardin, G., Halmi, M. and Raveau, B., *Sintering of various perovskites with lithium salts*. 6th CIMTEC, World Congress on Hightech Ceramics, 1986.
14. Haussonne, J. M. and Desgardin, G., Dielectric properties of barium titanate based capacitors with lithium additions. *Dielec tric Ceramics*, 1992, 155 165.